

# Analyst

Accepted Manuscript



This is an *Accepted Manuscript*, which has been through the Royal Society of Chemistry peer review process and has been accepted for publication.

*Accepted Manuscripts* are published online shortly after acceptance, before technical editing, formatting and proof reading. Using this free service, authors can make their results available to the community, in citable form, before we publish the edited article. We will replace this *Accepted Manuscript* with the edited and formatted *Advance Article* as soon as it is available.

You can find more information about *Accepted Manuscripts* in the [Information for Authors](#).

Please note that technical editing may introduce minor changes to the text and/or graphics, which may alter content. The journal's standard [Terms & Conditions](#) and the [Ethical guidelines](#) still apply. In no event shall the Royal Society of Chemistry be held responsible for any errors or omissions in this *Accepted Manuscript* or any consequences arising from the use of any information it contains.

1  
2  
3 **Investigating the relationship between changes of collagen fiber orientation**  
4  
5 **during skin aging and collagen/water interactions by polarized-FTIR**  
6  
7  
8 **microimaging**  
9

10  
11  
12  
13  
14  
15  
16 **Christophe Eklouh-Molinier,<sup>a,b</sup> Teddy Happillon,<sup>a,b</sup> Nicole Bouland,<sup>b,c</sup>**

17  
18  
19 **Caroline Fichel,<sup>b,c</sup> Marie-Danièle Diébold,<sup>b,c</sup> Jean-François Angiboust,<sup>a,b</sup>**

20  
21  
22 **Michel Manfait,<sup>a,b</sup> Sylvie Brassart-Pasco,<sup>b,d</sup> and Olivier Piot<sup>a,b,e\*</sup>**  
23  
24  
25  
26  
27

28 <sup>a</sup>Equipe MéDIAN-Biophotonique et Technologies pour la Santé, UFR de Pharmacie, Université de  
29  
30 Reims Champagne-Ardenne, Reims, France

31  
32 <sup>b</sup>CNRS UMR7369 MEDyC, SFR Cap-Santé, Reims, France

33  
34 <sup>c</sup>Laboratoire d'Anatomie et Cytologie Pathologiques, UFR Médecine, Université de Reims  
35  
36 Champagne-Ardenne, Reims, France

37  
38 <sup>d</sup>Laboratoire de Biochimie et de Biologie Moléculaire, UFR Médecine, Université de Reims  
39  
40 Champagne-Ardenne, Reims, France

41  
42 <sup>e</sup>Platform of Cellular and Tissular Imaging (PICT), Université de Reims Champagne-Ardenne, Reims,  
43  
44 France

45  
46  
47  
48  
49  
50 \*Address all correspondence to: Olivier Piot, Université de Reims Champagne-Ardenne,  
51  
52 Equipe MéDIAN-Biophotonique et Technologies pour la Santé, Unité MEDyC CNRS  
53  
54 UMR7369, UFR de Pharmacie, 51 rue Cognacq-Jay, 51096 Reims, France;  
55  
56  
57 Tel: +33 3 26 91 81 28; E-mail: [olivier.piot@univ-reims.fr](mailto:olivier.piot@univ-reims.fr)  
58  
59  
60

1  
2  
3 **Abstract.** Upon chronological aging, human skin undergoes structural and molecular  
4 modifications, especially at the level of type I collagen. This macromolecule is one of the  
5 main dermal structural proteins and presents several age-related alterations. It exhibits a triple  
6 helical structure and assembles itself to form fibrils and fibers. In addition, water plays an  
7 important role in stabilizing collagen triple helix by forming hydrogen-bonds between  
8 collagen residues. However, the influence of water on changes of dermal collagen fiber  
9 orientation with age is not been yet understood. Polarized-Fourier Transform Infrared (P-  
10 FTIR) imaging is an interesting biophotonic approach to determine *in situ* the orientation of  
11 type I collagen fibers, as we have recently shown by comparing skin samples of different  
12 ages. In this work, P-FTIR spectral imaging was performed on skin samples from two age  
13 groups (35- and 38-year-old on one hand, 60- and 66-year-old on the other hand); and our  
14 analyses were focused on the effect of H<sub>2</sub>O/D<sub>2</sub>O substitution. Spectral data were processed  
15 with fuzzy C-means (FCM) clustering in order to distinguish different orientations of collagen  
16 fibers. We demonstrated that the orientation was altered with aging, and that D<sub>2</sub>O treatment,  
17 affecting primarily highly bound water molecules, is more marked for youngest skin samples.  
18 Collagen-bound water-related spectral markers were also highlighted. Our results suggest a  
19 weakening of water/collagen interactions with age. This non-destructive and label-free  
20 methodology allows to understand better the importance of bound water in collagen fiber  
21 orientation alterations occurring with skin aging. Obtaining such structural information could  
22 find benefits in dermatology as well as in cosmetics.  
23  
24  
25  
26  
27  
28  
29  
30  
31  
32  
33  
34  
35  
36  
37  
38  
39  
40  
41  
42  
43  
44  
45  
46  
47  
48  
49  
50  
51  
52  
53

54 Keywords: P-FTIR imaging, skin aging, collagen, water, hydrogen-deuterium exchange  
55  
56  
57  
58  
59  
60

## Introduction

Skin is the largest organ of the human body and has many important functions such as protection against external aggressions and thermoregulation. This cutaneous structure is composed of three layers: the epidermis, the dermis and the hypodermis. The dermis is made up of two sub-layers: the superficial or papillary dermis, and the deep or reticular dermis. This dense conjunctive tissue is constituted of fibrous proteins like collagen and elastic fibers, and of non-fibrous components like proteoglycans (PGs) and cells. Type I collagen represents about 80% of skin dry mass and confers to the skin its strength and its resilience. Type I collagen fibers are responsible of tensile properties of the skin; they are thin and poorly organized in the papillary dermis while thicker and well organized in the reticular dermis<sup>1</sup>.

During aging, skin undergoes several structural and molecular changes such as the appearance of wrinkles and the loss of elasticity. That is why it is the subject of much attention in dermatology as well as in cosmetology. Some studies reported an accelerated degradation and a decreased synthesis of type I collagen with age and that this loss of collagen leads to a dermal atrophy<sup>2, 3, 4</sup>. Furthermore, it has been demonstrated that the elastic fibers network was altered with aging<sup>5, 6</sup>. A loss of hydration due to changes in PGs content and localization was observed upon aging<sup>7</sup>.

Playing an important role in stabilizing collagen triple helix, water molecules form hydrogen-bonds between collagen residues<sup>8, 9</sup>. Xia et al. hypothesized that interactions between water molecules and PGs could influence the orientation of collagen fibers in the articular cartilage<sup>10</sup>. Besides, several recent studies using magnetic resonance imaging demonstrated that the articular cartilage presents a well-distinct anisotropy closely connected to collagen ultrastructure and, also that the interaction between water molecules and PGs could modulate the orientation of collagen fibers *via* the influence of bound water modifications<sup>11, 12</sup>. Indeed, water bound to collagen behaves differently than the bulk water

1  
2  
3 and is involved in the formation of hydrogen bonds and water bridges between collagen triple  
4  
5 helix residues<sup>13-15</sup>. Thus, it has been suggested that water molecules could have a crucial role  
6  
7 in the stabilization of the conformation and the packing of collagen fibers in the articular  
8  
9 cartilage<sup>16, 17</sup>.

10  
11 Biophotonic techniques are potential tools to assess the orientation of collagen fibers.  
12  
13 Polarized light microscopy (PLM) is one of the first developed techniques allowing  
14  
15 morphology studies on collagen-rich tissues<sup>18-20</sup>. Some studies on skin have employed  
16  
17 polarization sensitive-optical coherent tomography (PS-OCT) to reveal the molecular  
18  
19 orientation of collagen fibers exhibiting some anisotropic properties such as birefringence<sup>21-24</sup>.  
20  
21 Second harmonic generation (SHG) technique is another emerging technique to investigate  
22  
23 collagenous tissues by exploiting the specificity of collagen SHG signal. In addition,  
24  
25 polarization-resolved imaging measurements permitted to determine the spatial distribution of  
26  
27 the orientation of collagen fibers<sup>25-27</sup>. Fourier Transform infrared (FTIR) spectroscopy is a  
28  
29 vibrational technique which allows obtaining some structural information on oriented  
30  
31 molecules like type I collagen when this biophotonic approach is combined to polarization  
32  
33 measurements. Compared to previous techniques, FTIR has the advantage to probe the entire  
34  
35 molecular composition of a complex sample such as cutaneous tissue. Indeed, some studies  
36  
37 have shown the efficiency of this technique to compare collagen fiber orientation in normal  
38  
39 and pathological articular tissue<sup>28-33</sup>. Recently, our group highlighted some changes in the  
40  
41 orientation of dermal collagen with age by using polarized-FTIR (P-FTIR) imaging<sup>34</sup>.  
42  
43 However, to the best of our knowledge, no studies have yet investigated the importance of  
44  
45 water in collagen fiber orientation with skin aging.  
46  
47  
48  
49  
50

51  
52 In this work, skin samples from thirty- and sixty-years-old women were treated with  
53  
54 deuterium oxide (D<sub>2</sub>O) to determine the influence of the bound water molecules in changes of  
55  
56 collagen fiber orientation. Untreated and treated skin cryosections were analyzed by P-FTIR  
57  
58  
59  
60

1  
2  
3 imaging. Spectral data were processed by fuzzy C-means (FCM) clustering to define the  
4 different layers of the skin and the different types of collagen fiber orientation within the  
5 dermis. Moreover, discriminant vibrations related to collagen/water interactions were  
6 highlighted for the two different-age skin samples by using discriminant wavenumber  
7 selection algorithm.  
8  
9  
10  
11  
12

## 13 **Materials & Methods**

### 14 *Sample preparation*

15  
16  
17  
18  
19  
20  
21 Frozen abdominal skin samples were obtained from female Caucasian subjects in their thirties  
22 (35- and 38-year-old) and in their sixties (60- and 66-year-old), through BIOPREDIC  
23 International (Rennes, France) and were treated as described by Zhang et al. for H<sub>2</sub>O/D<sub>2</sub>O  
24 substitution<sup>9</sup>. Briefly, skin samples were immersed into 1 mL of distilled water for 24h and  
25 then into 1 mL of deuterium oxide (D<sub>2</sub>O, 99,9% isotopic purity, Sigma-Aldrich, France) for  
26 24h. The first period in water aims at saturating all the interaction sites of the skin samples.  
27  
28  
29  
30  
31  
32  
33  
34  
35

36 Skin samples from the same age groups were also immersed into distilled water for 48h as  
37 controls. Control and deuterated samples were embedded in Tissue-Tek O.C.T. compound  
38 (Sakura Finetek, France) and were immediately snap frozen in liquid nitrogen. Five thin serial  
39 tissue cryosections (5 μm) were deposited on calcium fluoride (CaF<sub>2</sub>) windows. Hematoxylin  
40 and eosin (H&E) staining was used as standard staining on adjacent skin sections (5 μm) to  
41 those dedicated to FTIR analysis. Three 5 μm-thick sections of rat-tail tendons (Sprague-  
42 Dawley rats aged 2 months) were prepared according to the same protocol than skin samples.  
43  
44  
45  
46  
47  
48  
49  
50  
51

### 52 *Polarized-FTIR imaging*

1  
2  
3 Spectral data were collected by using a Vertex 70 FTIR spectrometer coupled to a  
4 HYPERION 3000 FTIR microscope (Bruker Optics, Ettlingen, Germany) controlled by the  
5 Opus 7.2 software and equipped with a 64x64 pixel Focal Plane Array (FPA) detector. FTIR  
6 spectral acquisitions were realized in transmission mode with a x15 Cassegrain objective and  
7 matching condenser lens. Cryosections of rat-tail tendon were aligned along the direction of  
8 x-axis of the motorized plate and spectral maps of 175x175  $\mu\text{m}^2$  were acquired in non-  
9 polarized mode and with IR radiation polarized perpendicular to the tendon orientation (*i.e.*,  
10 x-axis direction). In such material, the collagen fibers are arranged and aligned longitudinally  
11 to the tendon length. For each skin cryosections, a final measuring area of 175x350  $\mu\text{m}^2$   
12 mapped from the *stratum corneum* to the reticular dermis with a resolution of 2.7  $\mu\text{m}^2/\text{pixel}$ . It  
13 took about 3 minutes to record 8192 spectra. Polarization measurements were performed by  
14 inserting a polarizer in the incident IR beam. FPA imaging maps (n=5) were acquired for each  
15 tissue section whose the skin surface was oriented parallel to the x-axis of the motorized plate.  
16 To determine the spatial distribution of the collagen orientation, the polarization was chosen  
17 perpendicular to the skin surface. Each spectrum was recorded with 64 scans at a resolution of  
18 4  $\text{cm}^{-1}$ , on the 900-3800  $\text{cm}^{-1}$  spectral range. A background spectrum was recorded with 128  
19 scans of accumulation on a blank part of the same  $\text{CaF}_2$  window prior to spectral acquisitions.  
20 Each spectrum was rationed to the background spectrum in order to reduce any atmospheric  
21 effects and to obtain chemical features from the analyzed sample.  
22  
23  
24  
25  
26  
27  
28  
29  
30  
31  
32  
33  
34  
35  
36  
37  
38  
39  
40  
41  
42  
43  
44  
45  
46

#### 47 *Data analysis*

48  
49 Spectral data were preprocessed by an automated method based on Extended Multiplicative  
50 Signal Correction (EMSC) algorithm<sup>35</sup> implemented in the MATLAB 8.3 software (The  
51 Mathworks, USA). Briefly, EMSC allows to eliminate low signal/noise ratio spectra and to  
52 realize a baseline correction and normalization in order to compare spectra each other<sup>36, 37</sup>.  
53  
54  
55  
56  
57  
58  
59  
60

1  
2  
3 Subsequently, FCM clustering was used as statistical multivariate processing. FCM  
4 allows to assign each spectrum to every clusters with associated membership values  
5 comprised between 0 (no class membership) and 1 (highest degree of cluster membership)<sup>38</sup>.  
6  
7 Consequently, a spectrum could belong to several clusters contrary to “hard” clustering  
8 techniques such as K-Means<sup>39</sup>. FCM images were constructed with redundancy-based  
9 algorithm (RBA) that presents the advantage to determine automatically the number of  
10 clusters<sup>38-40</sup>. FCM clustering were performed using home-made algorithms written in the  
11  
12  
13  
14  
15  
16  
17  
18  
19  
20  
21  
22  
23  
24  
25  
26  
27  
28  
29  
30  
31  
32  
33  
34  
35  
36  
37  
38  
39  
40  
41  
42  
43  
44  
45  
46  
47  
48  
49  
50  
51  
52  
53  
54  
55  
56  
57  
58  
59  
60

20 The randfeatures function was used to identify the most discriminant wavenumbers  
21 between 2 groups of spectral data<sup>42-44</sup>. This algorithm, based on a random selection of a pool  
22 of 15 wavenumbers, reduces the spectra dimension (751 wavenumbers in our case) to the 15  
23 wavenumbers previously selected. Then, each spectrum is mean-centered by the subtraction  
24 of the mean spectrum of its group. A linear and supervised classification algorithm is then  
25 applied and returns, for each spectrum, a membership value towards each spectral group. A  
26 spectrum will be considered as well classified if its biggest membership value is attributed to  
27 the good category and if this value is over a Confidence Threshold (fixed in our case to 95%).  
28  
29 The last step deals with the number of spectra well classified, according to the previous  
30 conditions. If this classification is over a Performance Threshold (fixed here to 95%), the  
31 subset of 15 wavenumbers randomly selected is considered as efficient for the distinction  
32 between the two spectral groups, and thus a corresponding score is incremented by one for  
33 each wavenumber. This procedure is then repeated with another random selection of 15  
34 wavenumbers. It must be noted that a wavenumber can be chosen several times. The  
35 randfeatures function stops when 1000 subsets are retained. Finally, the scores of every  
36 wavenumbers can be analyzed by the user. Higher is a score, the more discriminant is the  
37  
38  
39  
40  
41  
42  
43  
44  
45  
46  
47  
48  
49  
50  
51  
52  
53  
54  
55  
56  
57  
58  
59  
60

1  
2  
3 corresponding wavenumber. This discriminant wavenumber selection algorithm was written  
4  
5 in the MATLAB 8.3 software.  
6  
7

## 8 9 **Results**

### 10 *P-FTIR spectral data analysis on rat-tail tendons*

11  
12 As previously realized in other studies<sup>18, 34</sup>, rat-tail tendon was used as a reference sample to  
13  
14 measure the effect of polarization on type I collagen IR signal. Reconstructed images and  
15  
16 mean spectra revealed a change in the Amide I/Amide II ratio as a function of the polarization  
17  
18 mode used. The Amide I/Amide II ratio presented a value of 1.4 without polarization, and  
19  
20 between 1.6 and 2 when the polarized IR radiation was perpendicular to the collagen fiber  
21  
22 orientation probing mainly stretching vibration of C=O bands as shown in Fig. S1 (Supporting  
23  
24 Information). Indeed, the C=O stretching, the major vibration of the Amide I band, displays a  
25  
26 transition moment preferentially oriented perpendicular to the collagen fiber long axis. Also,  
27  
28 the C-N stretching and the N-H bending, which contribute to the Amide II band, possess a  
29  
30 transition moment preferentially oriented parallel to the collagen fiber long axis. [rajouter les  
31  
32 réf] Thus, the Amide I/Amide II ratio is a potential indicator of the orientation of collagen  
33  
34 fibers, as probed by P-FTIR, and was used for next analyses on skin samples.  
35  
36  
37  
38  
39  
40  
41  
42

### 43 *P-FTIR spectral data analysis on human skin samples*

44  
45 Fig. 1(a) and 1(b) display H&E stained histological sections of the 35-year-old human skin  
46  
47 sample, untreated and treated with D<sub>2</sub>O respectively. These morphological images permitted  
48  
49 to visualize the main skin structures which are the epidermis and the dermis. Adjacent  
50  
51 sections were analyzed by FTIR imaging in a label-free manner. The presence of the 1338 cm<sup>-1</sup>  
52  
53 vibration referred to the collagen integrity, showed that collagen were not degraded during  
54  
55 treatment for all skin samples (data not shown)<sup>45, 46</sup>. Corresponding spectral FTIR images  
56  
57  
58  
59  
60

1  
2  
3 were constructed using the Amide I/Amide II integrated intensities ratio for the non-polarized  
4 [Fig. 1(c) and 1(d)] and for the perpendicular polarization [Fig. 1(e) and 1(f)]. By comparing  
5 the images collected in non-polarized mode with those acquired in perpendicular polarization,  
6 it is noteworthy that the polarization of IR signal increased markedly the Amide I/Amide II  
7 ratio, permitting to enhance the image contrast and to reveal an orientation of the peptide  
8 bonds of the protein components (*i.e.*, mainly collagen) of the skin. Compared to the values  
9 obtained from tendon analyses, the color-scale was adjusted from 1 (blue) to 2 (red). Three  
10 categories of orientation can be distinguished: Amide I/Amide II ratio  $\geq 1.6$  corresponds to  
11 collagen fibers oriented parallel to the skin surface, and  $\leq 1.3$  to those oriented perpendicular  
12 to the skin surface. A value between 1.3 and 1.6 could be associated to an oblique orientation  
13 of collagen fibers. The same methodology was also applied for the 38-, 60- and 66-year-old  
14 human skin samples, untreated [Fig. S2(a, c, e), Fig. S3(a, c, e) and Fig. S4(a, c, e)] and  
15 treated with D<sub>2</sub>O [Fig. S2(b, d, f), Fig. S3(b, d, f) and Fig. S4(b, d, f)] (Supporting  
16 Information).

33  
34  
35  
36 *Redundancy-based algorithm (RBA)-fuzzy C-means (FCM) clustering on FTIR spectral*  
37 *images*

38  
39  
40 In order to distinguish more precisely the different regions of the dermis, RBA-FCM  
41 clustering was performed to the perpendicular polarized FTIR data acquired from 35-year-old  
42 human skin sections, untreated and treated with D<sub>2</sub>O (Fig. 2). The same processing was  
43 applied on 38-, 60- and 66-year-old human skin sections, treated or not with D<sub>2</sub>O (Fig. S5, S6  
44 and S7 in Supporting Information). With this automatic clustering, the cluster #1 represents  
45 the epidermis and clusters #2, 3, 4 and 5 are associated to the dermis. By comparing these  
46 latter images with those created from the Amide I/Amide II ratio, it appears that the clusters  
47 corresponding to dermis match quite well to different categories of collagen orientation. Thus,  
48  
49  
50  
51  
52  
53  
54  
55  
56  
57  
58  
59  
60

1  
2  
3 the cluster #2 can be associated to collagen fibers oriented parallel to the skin surface and,  
4  
5 conversely, collagen fibers oriented perpendicular to the skin surface correspond to the cluster  
6  
7 #4. Collagen fibers with an oblique orientation are found in the cluster #3. Presenting a  
8  
9 marked spatial dispersion of pixels for all skin sections, having a low signal-to-noise ratio and  
10  
11 being minority with regard to other clusters, the cluster #5 was not considered in the  
12  
13 following results.  
14  
15

16  
17 Table 1 summarizes the spatial repartition (in terms of relative proportion of pixels) of  
18  
19 each orientation (parallel, perpendicular and oblique) of collagen fibers for different-age  
20  
21 human skin samples, treated or not with D<sub>2</sub>O. Values were averaged on 5 cryosections for  
22  
23 each skin sample. For the 35- and 38-year-old skin samples, results show an increase (from  
24  
25 25.1% to 34.3%) of the proportion of perpendicular orientations of collagen fibers (cluster  
26  
27 #4), a decreasing trend (38.2% to 27.5%) of the proportion of oblique orientations (cluster  
28  
29 #3), and no significant changes for parallel orientations (cluster #2) with D<sub>2</sub>O treatment. For  
30  
31 the 60- and 66-year-old skin samples, no significant changes associated to the D<sub>2</sub>O treatment  
32  
33 are noticed for any orientation of collagen fibers.  
34  
35  
36  
37

#### 38 *Collagen-bound water-related spectral markers from different-age skin samples*

39  
40 In order to identify vibrations associated to changes of collagen fiber orientation, extracted  
41  
42 spectra from the cluster #4 (perpendicular oriented collagen fibers) of different-age and –  
43  
44 treatment of skin samples were compared using the randfeatures algorithm. Due to significant  
45  
46 differences as previously presented in Table 1, only the cluster #4 was considered in this  
47  
48 analysis. A selection of 3000 spectra, extracted from the 5 different cryosections for each skin  
49  
50 sample and equally distributed between the untreated and the D<sub>2</sub>O-treated skin samples, was  
51  
52 performed. Fixing a score > 30, 11 and 8 most discriminant wavenumbers were retained  
53  
54 respectively for the 35-year-old [Fig. 4(a)] and for the 66-year-old skin samples [Fig. 4(b)],  
55  
56  
57  
58  
59  
60

1  
2  
3 and were arranged in the form of spectral color barcode according to the discrimination level  
4  
5 of the scores. The same procedure was also applied on 38- and 60-year-old human skin  
6  
7 sections, giving similar results (Fig. S8 in Supporting Information). The color codes were  
8  
9 used as followed: *orange* for the less discriminant wavenumbers (scores between 30 and 33);  
10  
11 *brown* for the intermediate discriminant (scores between 34 and 36); and *red* for the most  
12  
13 discriminant (scores  $\geq 37$ ). It can be noted that 8 wavenumbers in  $1650\text{ cm}^{-1}$ ,  $1555\text{ cm}^{-1}$ ,  $1455$   
14  
15  $\text{cm}^{-1}$ ,  $1390\text{ cm}^{-1}$ ,  $1330\text{ cm}^{-1}$  and between  $1300$  and  $1200\text{ cm}^{-1}$ , were found common to the skin  
16  
17 types. They correspond mainly to the vibrations specific of proteins. Besides, three additional  
18  
19 discriminant wavenumbers in  $1120\text{ cm}^{-1}$ ,  $1080\text{ cm}^{-1}$  and  $1050\text{ cm}^{-1}$ , corresponding to  
20  
21 carbohydrates vibrations, were found exclusively in the young skin sample. Their peak  
22  
23 position and molecular attribution are summarized in Table 2.  
24  
25  
26  
27  
28

## 29 **Discussion**

30  
31 Understanding the interaction between dermal collagen network and its surrounding  
32  
33 environment is of interest to gain insight on molecular and functional changes undergone by  
34  
35 the cutaneous tissue during aging. Type I collagen is the main macromolecule of the dermis  
36  
37 able to form a fibrous network and is strongly involved in the mechanical properties of the  
38  
39 skin as well as in its hydration. Indeed, water plays a crucial role for maintaining the assembly  
40  
41 formed by collagen macromolecules. Most of water molecules are tightly bound to proteins  
42  
43 and consequently intervene in the skin microstructure. Apart these interacting water  
44  
45 molecules, there are water molecules, called bulk or tetrahedron water, not bound to proteins  
46  
47 but more likely bound to each other<sup>47</sup>. Treatment by heavy water is a way to investigate the  
48  
49 water/collagen interactions as previously used to observe changes of the collagen model  
50  
51 peptides stability and to highlight hydration forces between collagen triple helices<sup>48, 49</sup>. More  
52  
53 recently, other groups realized H/D exchange on different tissues such as skin, pericardium  
54  
55  
56  
57  
58  
59  
60

1  
2  
3 and bone in order to remove primarily water molecules bound to collagen fibers<sup>9, 50, 51</sup>.  
4  
5 Substitution of bound water molecules by D<sub>2</sub>O is possible due to the respective  
6  
7 thermodynamic properties of water and heavy water. Indeed, although these two molecules  
8  
9 have a similar size, deuterium bonds are stronger than hydrogen bonds with dissociation  
10  
11 energies of 6.53 kJ mol<sup>-1</sup> and 5.52 kJ mol<sup>-1</sup>, respectively, according to theoretical models<sup>52, 53</sup>.  
12  
13 In our study, the effect of H<sub>2</sub>O/D<sub>2</sub>O substitution was considered by studying the collagen  
14  
15 fibers orientation, structural information that can be probed within skin specimens by  
16  
17 exploiting the polarization of the IR radiation<sup>34, 41</sup>. Such changes of behavior of collagen  
18  
19 network observed between skins of different ages are very likely to be linked with a  
20  
21 degradation of the mechanical properties, whose one of the visible signs is the appearance of  
22  
23 wrinkles. Our approach relies on a quantification of the effect of H<sub>2</sub>O/D<sub>2</sub>O substitution on  
24  
25 collagen orientation by comparing skins from two different age groups.  
26  
27  
28

29  
30 A particular statistical clustering method (RBA-FCM) was used to overcome the  
31  
32 inconvenient of more classical techniques such as K-Means which the result is highly  
33  
34 dependent of the number of the clusters chosen by the operator. In RBA-FCM processing, the  
35  
36 number of clusters is automatically determined facilitating the comparison of samples since it  
37  
38 is not subject to the operator interpretation. Thus, distinct parts associated to different  
39  
40 orientations of collagen fibers were highlighted in the dermis: parallel (cluster #2), oblique  
41  
42 (cluster #3), and perpendicular (cluster #4) to the skin surface. It is worth noting that pixel  
43  
44 spatial distributions of parallel and perpendicular orientations appear to be packed, whereas  
45  
46 that of the oblique orientation seems to be sparse. Concerning the cluster associated to the  
47  
48 parallel oriented collagen fibers, the quantitative results were obtained by taking into account  
49  
50 both the papillary dermis and a part of the reticular dermis. The examination of the FCM  
51  
52 images (cluster #2) showed that the part corresponding to the papillary dermis decreases in  
53  
54  
55  
56  
57  
58  
59  
60

1  
2  
3 the samples of the oldest group, which is consistent with the loss of papillary dermal  
4  
5 compartment observed during aging<sup>54</sup>.  
6

7  
8         Thereafter, regarding the impact of D<sub>2</sub>O treatment, in the youngest skins, the H/D  
9  
10 exchange led to favor perpendicular orientation of collagen fibers at the expense of oblique  
11  
12 orientation. On the contrary, the D<sub>2</sub>O treatment appears to not affect significantly the  
13  
14 proportions of different orientations of collagen fibers in the old skin samples. These  
15  
16 observations could reflect differences between the age groups in the number of water  
17  
18 molecules bound to collagen and also in their interaction strength. It is hard to study in details  
19  
20 the involved molecular mechanisms; additional experimental approaches would be required to  
21  
22 assess thermodynamics behaviors of water molecules interacting with macromolecular  
23  
24 proteins by using for example dynamic vapor sorption and scanning electron microscopy to  
25  
26 study simultaneously the organization of collagen network at the nanoscale<sup>9, 55</sup>. Here, our  
27  
28 objective was humbly to show the sensitivity of FTIR imaging in highlighting specific  
29  
30 behaviors for skin samples of different ages. We focused our interpretation on the collagen  
31  
32 that is by far the main component of the dermis. We demonstrated from reference tendon  
33  
34 samples that P-FTIR is a very sensitive to probe collagen fibers orientation. However, another  
35  
36 macromolecular component, elastin, is known to be affected by ageing and also to be directly  
37  
38 involved in the skin mechanical properties<sup>56</sup> even though the elastic fiber network represents  
39  
40 only 5% of the dermis dry mass. By analyzing nuchal bovine ligament, we checked that FTIR  
41  
42 signal of elastin appeared to be much less sensitive to the polarization of the incident beam  
43  
44 than collagen (data not shown). Consequently, elastic fibers were not considered in our data  
45  
46 interpretation but it would deserve to bring attention to it, possibly by investigating their  
47  
48 spatial distribution thanks to their intrinsic fluorescent properties by using multiphoton  
49  
50 microscopy<sup>57</sup>.  
51  
52  
53  
54  
55  
56  
57  
58  
59  
60

1  
2  
3 In addition to determine the relative proportion of the different collagen fiber  
4 orientations, infrared wavenumbers affected by the D<sub>2</sub>O treatment were identified using  
5 statistical processing. Obviously, protein vibrations are pinpointed for the two age groups. But  
6  
7 interestingly, vibrations were highlighted in the 1000-1150 cm<sup>-1</sup> range for the youngest skin  
8  
9 samples. This latter spectral region is often associated to sugars originating from advanced  
10 glycation endproducts<sup>40, 58</sup>, from PGs<sup>29, 32</sup>, and in a much less extent to nucleic acids<sup>59, 60</sup>. As  
11  
12 PGs represent the major part of carbohydrates in the dermis, their interaction with collagen  
13  
14 fibers is very probably altered during the H/D exchange. These results are consistent with the  
15  
16 involvement of GAG in collagen hydration. Indeed, GAGs from PGs have a key-role in skin  
17  
18 regarding to their ability to bind up to 1000 times their volume in water, due to their high  
19  
20 polarity. Therefore, skin hydration is highly correlated to the content and distribution of  
21  
22 dermal GAGs<sup>61</sup>. Recently, Li et al. demonstrated that the size of GAG chain of decorin, the  
23  
24 most abundant PGs in human dermis, was reduced in sun-protected old skin compared to  
25  
26 young skin<sup>62</sup>. Alterations of this GAG entity of decorin could explain the lack of interaction  
27  
28 between water molecules and GAGs in old dermis skin and could contribute to skin fragility  
29  
30 of elderly people. Playing a crucial role in the hydration of collagen fibers, PGs could  
31  
32 therefore affect the structure but also the orientation of the collagen fibers in young skin. PGs  
33  
34 may less interact with collagen with age and consequently lead to a decrease in the hydration  
35  
36 of collagen fibers. This latter could be related to the changes of orientation of collagen fibers  
37  
38 demonstrated in our study.

39  
40  
41 In this study, various methodological approaches of sample preparation (heavy water  
42  
43 substitution), of data acquisition (polarization mode) or of data processing (automatic  
44  
45 clustering and discriminant wavenumbers selection), were applied to investigate alterations of  
46  
47 the dermis associated to the chronological aging at the molecular level. Similar approaches  
48  
49 could be used in other issues without complicated adaptation, such as in the context of photo-

1  
2  
3 aging where water structure and interactions with proteins and GAGs were demonstrated by  
4  
5 Gniadecka et al.<sup>63</sup> to be altered in photo-aged skins; and also in more medical issues such as  
6  
7 age-related diseases like diabetes. In addition, they could be of interest the characterization of  
8  
9 skin cancer, as shown in a recent study reporting that the *in vivo* determination of water  
10  
11 content by using vibrational Raman spectroscopy may contribute to differentiate between  
12  
13 tumor and healthy tissue<sup>64</sup>.  
14  
15  
16  
17

## 18 **Conclusion**

19  
20 This study exhibits the potential of P-FTIR microimaging associated to advanced statistical  
21  
22 clustering methods to probe changes of collagen fibers orientations between skin samples of  
23  
24 different ages. Recent devices equipped with FPA matricial detectors make feasible in routine  
25  
26 use of the technique by reducing considerably the acquisition time of tissue samples. D<sub>2</sub>O  
27  
28 treatment affects significantly only the youngest skin samples, quite possible *via* PG  
29  
30 involvement. This methodology is promising for a better insight on relationship between  
31  
32 water molecules and collagen fiber organization upon chronological aging, bringing a  
33  
34 potential added value as well in cosmetics as in dermatology.  
35  
36  
37  
38  
39

## 40 **Acknowledgements**

41  
42 C. Eklouh-Molinier is a recipient of a doctoral fellowship of the Région Champagne-Ardenne.  
43  
44 The authors would like to thank the Région Champagne-Ardenne (projet Emergence) and the  
45  
46 Plateform of Cellular and Tissular Imaging (PICT) for the equipment availability.  
47  
48  
49  
50

## 51 **References**

- 52  
53  
54  
55 1. F. H. Silver, J. W. Freeman, and D. DeVore, *Skin Res. Technol.*, 2001, **7**, 18–23.  
56  
57  
58  
59  
60

- 1  
2  
3 2. S. Shuster, M. M. Black, and E. McVitie, *Br J Dermatol*, 1975, **93**, 639–643.
- 4  
5  
6 3. C. Escoffier, J. de Rigal, A. Rochefort, R. Vasselet, J. L. Leveque, and P. G. Agache, *J*  
7  
8  
9  
10  
11  
12  
13  
14  
15  
16  
17  
18  
19  
20  
21  
22  
23  
24  
25  
26  
27  
28  
29  
30  
31  
32  
33  
34  
35  
36  
37  
38  
39  
40  
41  
42  
43  
44  
45  
46  
47  
48  
49  
50  
51  
52  
53  
54  
55  
56  
57  
58  
59  
60  
14. R. Z. Kramer, L. Vitagliano, J. Bella, R. Berisio, L. Mazzarella, B. Brodsky, A. Zagari,  
and H. M. Berman, *J. Mol. Biol.*, 1998, **280**, 623–638.
11. Y. Xia, *Magn. Reson. Med.*, 1998, **39**, 941–949.
10. Y. Xia, J. B. Moody, N. Burton-Wurster, and G. Lust, *Osteoarthr. Cartil.*, 2001, **9**,  
393–406.
9. Q. Zhang, K. L. Andrew Chan, G. Zhang, T. Gillece, L. Senak, D. J. Moore, R.  
Mendelsohn, and C. R. Flach, *Biopolymers*, 2011, **95**, 607–615.
8. J. Bella, B. Brodsky, and H.M. Berman, *Structure*, 1995, **3**, 893-906.
7. D.A. Carrino, J.M. Sorrell, and A.I. Caplan, *Arch Biochem Biophys*, 2000, **373**, 91-101.
6. S. Imayama, and I.M. Braverman, *Am J Pathol*, 1989, **134**, 1019-25.
5. I. Pasqueli-Ronchetti, and M. Baccarani-Contri, *Microsc Res Tech*, 1997, **38**, 428-435.
4. L. Rittié, and G.J. Fisher, *Ageing Res Rev*, 2002, **1**, 705-720.
3. C. Escoffier, J. de Rigal, A. Rochefort, R. Vasselet, J. L. Leveque, and P. G. Agache, *J*  
*Invest Dermatol*, 1989, **93**, 353–357.
2. S. Shuster, M. M. Black, and E. McVitie, *Br J Dermatol*, 1975, **93**, 639–643.

- 1  
2  
3 15. G. Melacini, A. M. Bonvin, M. Goodman, R. Boelens, and R. Kaptein, *J. Mol. Biol.*,  
4 2000, **300**, 1041–49.  
5  
6  
7  
8 16. I. G. Mogilner, G. Ruderman, and J. R. Grigera, *J. Mol. Graph. Model.*, 2002, **21**, 209–  
9 213.  
10  
11  
12  
13 17. L. V. Krasnosselskaia, G. D. Fullerton, S. J. Dodd, and I. L. Cameron, *Magn. Reson.*  
14 *Med.*, 2005, **54**, 280–288.  
15  
16  
17  
18 18. X. Bi, G. Li, S. B. Doty, and N. P. Camacho, *Osteoarthr. Cartil.*, 2005, **13**, 1050–8.  
19  
20  
21  
22 19. S. K. de Visser, J. C. Bowden, E. Wentrup-Byrne, L. Rintoul, T. Bostrom, J. M. Pope,  
23 and K. I. Momot, *Osteoarthr. Cartil.*, 2008, **16**, 689–697.  
24  
25  
26  
27 20. J. F. Ribeiro, E. H. M. dos Anjos, M. L. S. Mello, and B. de Campos Vidal, *PLoS One*,  
28 2013, **8**, 54724.  
29  
30  
31 21. C. E. Saxer, J. F. de Boer, B. H. Park, Y. Zhao, Z. Chen, and J. S. Nelson, *Opt. Lett.*,  
32 2000, **25**, 1355–7.  
33  
34  
35 22. M. C. Pierce, J. Strasswimmer, B. H. Park, B. Cense, and J. F. de Boer, *J Invest*  
36 *Dermatol*, 2004, **123**, 458–463.  
37  
38  
39 23. S. Sakai, M. Yamanari, A. Miyazawa, M. Matsumoto, N. Nakagawa, T. Sugawara, K.  
40 Kawabata, T. Yatagai, and Y. Yasuno, *J. Invest. Dermatol.*, 2008, **128**, 1641–47.  
41  
42  
43  
44 24. S. Sakai, M. Yamanari, Y. Lim, N. Nakagawa, and Y. Yasuno, *Biomed. Opt. Express*,  
45 2011, **2**, 2623.  
46  
47  
48  
49  
50  
51 25. R. M. Williams, W. R. Zipfel, and W. W. Webb, *Biophys. J.*, 2005, **88**, 1377–86.  
52  
53  
54  
55  
56  
57  
58  
59  
60

- 1  
2  
3 26. I. Gusachenko, G. Latour, and M.-C. Schanne-Klein, *Opt. Express*, 2010, **18**, 19339–  
4 52.  
5  
6  
7  
8 27. I. Gusachenko, V. Tran, Y. G. Houssen, J. M. Allain, and M. C. Schanne-Klein,  
9 *Biophys. J.*, 2012, **102**, 2220–29.  
10  
11  
12  
13 28. N. Ramakrishnan, Y. Xia, and A. Bidthanapally, *Phys. Med. Biol.*, 2007, **52**, 4601–14.  
14  
15  
16  
17 29. Y. Xia, N. Ramakrishnan, and A. Bidthanapally, *Osteoarthr. Cartil.*, 2007, **15**, 780–  
18 788.  
19  
20  
21  
22 30. X. Bi, X. Yang, M. P. G. Bostrom, D. Bartusik, S. Ramaswamy, K. W. Fishbein, R. G.  
23 Spencer, and N. P. Camacho, *Anal. Bioanal. Chem.*, 2007, **387**, 1601–12.  
24  
25  
26  
27  
28 31. N. Ramakrishnan, Y. Xia, and A. Bidthanapally, *J. Orthop. Surg. Res.*, 2008, **3**, 48.  
29  
30  
31  
32 32. J. H. Yin, Y. Xia, and N. Ramakrishnan, *Vib. Spectrosc.*, 2011, **57**, 338–341.  
33  
34  
35 33. J. H. Lee, and Y. Xia, *Microsc. Res. Tech.*, 2013, **76**, 625–632.  
36  
37  
38 34. T. T. Nguyen, C. Eklouh-Molinier, D. Sebiskveradze, J. Feru, C. Terryn, M. Manfait,  
39 S. Brassart-Pasco, and O. Piot, *Analyst*, 2014, **139**, 2482–8.  
40  
41  
42  
43 35. A. Kohler, C. Kirschner, A. Oust, and H. Martens, *Appl. Spectrosc.*, 2005, **59**, 707–  
44 716.  
45  
46  
47  
48  
49 36. E. Ly, O. Piot, R. Wolthuis, A. Durlach, P. Bernard, and M. Manfait, *Analyst*, 2008,  
50 **133**, 197–205.  
51  
52  
53  
54  
55 37. J. Nallala, O. Piot, M.-D. Diebold, C. Gobinet, O. Bouche, M. Manfait, and G. D.  
56 Sockalingum, *Cytometry. A*, 2013, **83**, 294–300.  
57  
58  
59  
60

- 1  
2  
3 38. D. Sebiskveradze, V. Vrabie, C. Gobinet, A. Durlach, P. Bernard, E. Ly, M. Manfait, P.  
4  
5 Jeannesson, and O. Piot, *Lab. Investig.*, 2011, **91**, 799–811.  
6  
7  
8  
9 39. S. M. Ali, F. Bonnier, K. Ptasinski, H. Lambkin, K. Flynn, F. M. Lyng and H. J. Byrne,  
10  
11 *Analyst*, 2013, **138**, 3946–56.  
12  
13  
14 40. M. Guilbert, C. Eklouh-Molinier, K. Wehbe, J. Sulé-Suso, Y. Yang, G. Cinque, P.  
15  
16 Jeannesson, and G. D. Sockalingum, *J. Biomed. Opt.*, 2014, **19**, 111612.  
17  
18  
19 41. C. Eklouh-Molinier, T. T. Nguyen, D. Sebiskveradze, J. Feru, N. Bouland, C. Terryn,  
20  
21 M. Manfait, S. Brassart-Pasco, and O. Piot, *Biomedical Spectroscopy and Imaging*,  
22  
23 2014, **3**, 281–286.  
24  
25  
26  
27 42. H. Liu, and H. Motoda, *Feature Selection for Knowledge Discovery and Data Mining*,  
28  
29 Kluwer Academic Publishers: Norwell, MA, USA, 1998.  
30  
31  
32  
33 43. D. T. Ross, U. Scherf, M. B. Eisen, C. M. Perou, C. Rees, P. Spellman, V. Iyer, S. S.  
34  
35 Jeffrey, M. Van de Rijn, M. Waltham, A. Pergamenschikov, J. C. Lee, D. Lashkari, D.  
36  
37 Shalon, T. G. Myers, J. N. Weinstein, D. Botstein, and P. O. Brown, *Nat Genet*, 2000,  
38  
39 **24**, 227–235.  
40  
41  
42  
43 44. T. T. Nguyen, T. Happillon, J. Feru, S. Brassart-Passco, J. F. Angiboust, M. Manfait,  
44  
45 and O. Piot, *J. Raman Spectrosc.*, 2013, **44**, 1230–37.  
46  
47  
48  
49 45. M. Jackson, L.P. Choo, P.H. Watson, W.C. Halliday, and H.H Mantsch, *Biochim*  
50  
51 *Biophys Acta*, 1995, **1270**, 1-6.  
52  
53  
54 46. P.A. West, P.A. Torzilli, C. Chen, P. Lin, and N.P. Camacho, *J Biomed Opt.*, 2005, **10**,  
55  
56 14015.  
57  
58  
59  
60

- 1  
2  
3 47. M. Gniadecka, O. F. Nielsen, D. H. Christensen, and H. C. Wulf, *J. Invest. Dermatol.*,  
4  
5 1998, **110**, 393–398.  
6  
7  
8 48. K. Mizuno, and H. P. Bächinger, *Biopolymers*, 2010, **93**, 93–101.  
9  
10  
11 49. S. Leikin, V. A. Parsegian, W. Yang, and G. E. Walrafen, *Proc. Natl. Acad. Sci. U. S.*  
12  
13 *A.*, 1997, **94**, 11312–17.  
14  
15  
16  
17 50. M. Jastrzebska, R. Wrzalik, A. Kocot, J. Zalewska-Rejdek, and B. Cwalina, *J.*  
18  
19 *Biomater. Sci. Polym. Ed.*, 2003, **14**, 185–197.  
20  
21  
22 51. M. Unal, S. Yang, and O. Akkus, *Bone*, 2014, **67**, 228–236.  
23  
24  
25  
26 52. G. Nemethy, and H. A. Scheraga, *J. Chem. Phys.*, 1962, **36**, 3382.  
27  
28  
29 53. G. Nemethy, and H. A. Scheraga, *J. Chem. Phys.*, 1964, **41**, 680-689.  
30  
31  
32 54. D. G. Janson, G. Saintigny, A. van Adrichem, C. Mahé, and A. El Ghalbzouri, *J.*  
33  
34 *Invest. Dermatol.*, 2012, **132**, 2565–72.  
35  
36  
37 55. C.R. Lovell, K.A. Smolenski, V.C. Duance, N.D. Light, S. Young, and M. Dyson, *Br.*  
38  
39 *J. Dermatol.*, 1987, **117**, 419-428.  
40  
41  
42  
43 56. V.L. Chen, R. Fleischmajer, E. Schwartz, M. Palaia, and R. Timpl, *J. Invest.*  
44  
45 *Dermatol.*, 1986, **87**, 334-337  
46  
47  
48 57. J.-C. Pittet, O. Freis, M.-D. Vazquez-Duchêne, G. Périé and G. Pauly, *Cosmetics*, 2014,  
49  
50 **1**, 211–221.  
51  
52  
53  
54 58. G. Birarda, E. Holman, S. Fu, and K. Weikel, *Biomedical Spectroscopy and Imaging*,  
55  
56 2013, **2**, 301–315.  
57  
58  
59  
60

- 1  
2  
3 59. S. E. Holton, M. J. Walsh, A. Kajdacsy-Balla, and R. Bhargava, *Biophys. J.*, 2011, **101**,  
4 1513–21.  
5  
6  
7  
8 60. D. R. Whelan, K. R. Bambery, P. Heraud, M. J. Tobin, M. Diem, D. McNaughton, and  
9 B. R. Wood, *Nucleic Acids Res.*, 2011, **39**, 5439–48.  
10  
11  
12  
13 61. E. F. Bernstein, C. B. Underhill, P. J. Hahn, D. B. Brown, and J. Uitto, *Br. J.*  
14 *Dermatol.*, 1996, **135**, 255–262.  
15  
16  
17  
18 62. Y. Li, Y. Liu, W. Xia, D. Lei, J. J. Voorhees, and G. J. Fisher, *Sci. Rep.*, 2013, **3**, 2422.  
19  
20  
21  
22  
23 63. M. Gniadecka, O. F. Nielsen, S. Wessel, M. Heidenheim, D. H. Christensen, and H. C.  
24 Wulf, *J. Invest. Dermatol.*, 1998, **111**, 1129–33.  
25  
26  
27  
28 64. E. M. Barroso, R. W. H. Smits, T. C. Bakker Schut, I. Ten Hove, J. a Hardillo, E. B.  
29 Wolvius, R. J. Baatenburg de Jong, S. Koljenović and G. J. Puppels, *Anal. Chem.*,  
30 2015.  
31  
32  
33  
34  
35  
36  
37  
38  
39  
40  
41  
42  
43  
44  
45  
46  
47  
48  
49  
50  
51  
52  
53  
54  
55  
56  
57  
58  
59  
60

### Figures captions

**Figure 1:** FTIR imaging on 35-year-old skin sections treated or not with D<sub>2</sub>O. H&E stained adjacent tissue sections from untreated (**a**) and treated (**b**) skin sample. Corresponding Amide I/Amide II (integrated intensities: 1590-1720 cm<sup>-1</sup>/1480-1590 cm<sup>-1</sup>) ratio-based reconstructed FTIR images in the non-polarized mode (**c, d**) and with the perpendicular polarization (**e, f**). Scale bar = 50 μm.

**Figure 2:** FCM clustering on perpendicular polarized FTIR images from untreated (**a**) and treated with D<sub>2</sub>O (**b**) 35-year-old skin section. Assignment of the clusters: cluster 1 (epidermis); clusters 2, 3, 4 and 5 (dermis).

**Figure 3:** Discriminant wavenumbers identified by using randfeatures algorithm in perpendicular oriented collagen fibers, (a) between D<sub>2</sub>O-untreated (*in red*) and treated (*in blue*) 35-years-old dermal skin samples and (b) D<sub>2</sub>O-untreated (*in orange*) and treated (*in black*) 66-years-old dermal skin samples. Respective scores are indicated above color-coded discriminant wavenumbers according to their discrimination level (30-33: orange; 34-36: brown; ≥ 37: red).

**Figure S1:** FTIR imaging on rat-tail tendon section. Amide I/Amide II (integrated intensities: 1590-1720 cm<sup>-1</sup>/1480-1590 cm<sup>-1</sup>) ratio-based reconstructed FTIR images and mean spectra in the non-polarized mode (**a**) and with the perpendicular polarization (**b**).

**Figure S2:** FTIR imaging on 38-year-old skin sections treated or not with D<sub>2</sub>O. H&E stained adjacent tissue sections from untreated (**a**) and treated (**b**) skin sample. Corresponding Amide I/Amide II (integrated intensities: 1590-1720 cm<sup>-1</sup>/1480-1590 cm<sup>-1</sup>) ratio-based reconstructed

1  
2  
3 FTIR images in the non-polarized mode (**c, d**) and with the perpendicular polarization (**e, f**).

4  
5 Scale bar = 50  $\mu\text{m}$ .

6  
7  
8  
9  
10 **Figure S3:** FTIR imaging on 60-year-old skin sections treated or not with D<sub>2</sub>O. H&E stained  
11 adjacent tissue sections from untreated (**a**) and treated (**b**) skin sample. Corresponding Amide  
12 I/Amide II (integrated intensities: 1590-1720  $\text{cm}^{-1}$ /1480-1590  $\text{cm}^{-1}$ ) ratio-based reconstructed  
13 FTIR images in the non-polarized mode (**c, d**) and with the perpendicular polarization (**e, f**).

14  
15  
16 Scale bar = 50  $\mu\text{m}$ .

17  
18  
19  
20  
21  
22  
23 **Figure S4:** FTIR imaging on 66-year-old skin sections treated or not with D<sub>2</sub>O. H&E stained  
24 adjacent tissue sections from untreated (**a**) and treated (**b**) skin sample. Corresponding Amide  
25 I/Amide II (integrated intensities: 1590-1720  $\text{cm}^{-1}$ /1480-1590  $\text{cm}^{-1}$ ) ratio-based reconstructed  
26 FTIR images in the non-polarized mode (**c, d**) and with the perpendicular polarization (**e, f**).

27  
28  
29 Scale bar = 50  $\mu\text{m}$ .

30  
31  
32  
33  
34  
35  
36 **Figure S5:** FCM clustering on perpendicular polarized FTIR images from untreated (**a**) and  
37 treated with D<sub>2</sub>O (**b**) 38-year-old skin section. Assignment of the clusters: cluster 1  
38 (epidermis); clusters 2, 3, 4 and 5 (dermis).

39  
40  
41  
42  
43  
44  
45 **Figure S6:** FCM clustering on perpendicular polarized FTIR images from untreated (**a**) and  
46 treated with D<sub>2</sub>O (**b**) 60-year-old skin section. Assignment of the clusters: cluster 1  
47 (epidermis); clusters 2, 3, 4 and 5 (dermis).

1  
2  
3 **Figure S7:** FCM clustering on perpendicular polarized FTIR images from untreated (**a**) and  
4 treated with D<sub>2</sub>O (**b**) 66-year-old skin section. Assignment of the clusters: cluster 1  
5 (epidermis); clusters 2, 3, 4 and 5 (dermis).  
6  
7  
8

9  
10  
11 **Figure S8:** Discriminant wavenumbers identified by using randfeatures algorithm in  
12 perpendicular oriented collagen fibers, (a) between D<sub>2</sub>O-untreated (*in red*) and treated (*in*  
13 *blue*) 38-years-old dermal skin samples and (b) D<sub>2</sub>O-untreated (*in orange*) and treated (*in*  
14 *black*) 60-years-old dermal skin samples. Respective scores are indicated above color-coded  
15 discriminant wavenumbers according to their discrimination level (30-33: orange; 34-36:  
16 brown; ≥ 37: red).  
17  
18  
19  
20  
21  
22  
23  
24  
25  
26

### 27 **Tables captions**

28  
29 **Table 1:** Quantitative analysis of different orientations (parallel, oblique and perpendicular)  
30 of collagen fibers in the different-age skin samples, untreated (- D<sub>2</sub>O) and treated (+ D<sub>2</sub>O)  
31 with D<sub>2</sub>O. The percentages were calculated from the number of pixels in the clusters  
32 associated to the different orientations. Standard deviations were obtained after averaging data  
33 collected on 5 analyzed sections for each skin sample.  
34  
35  
36  
37  
38  
39  
40  
41

42 **Table 2:** FTIR spectral peak attributions.  
43  
44  
45  
46  
47  
48  
49  
50  
51  
52  
53  
54  
55  
56  
57  
58  
59  
60

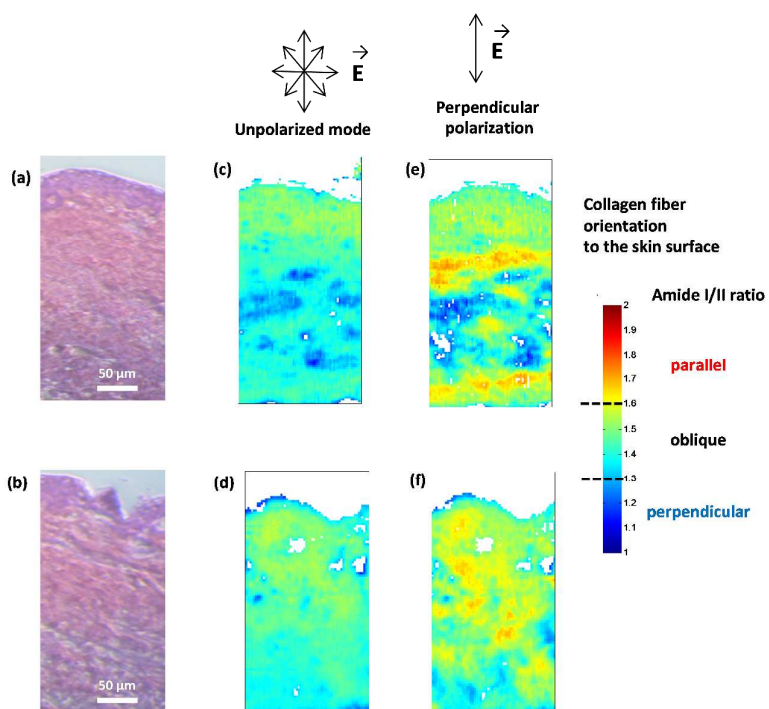


**Figure 1:** FTIR imaging on 35-year-old skin sections treated or not with D<sub>2</sub>O. H&E stained adjacent tissue sections from untreated (a) and treated (b) skin sample. Corresponding Amide I/Amide II (integrated intensities: 1590-1720 cm<sup>-1</sup>/1480-1590 cm<sup>-1</sup>) ratio-based reconstructed FTIR images in the non-polarized mode (c,d) and with the perpendicular polarization (e,f). Scale bar = 50 μm.

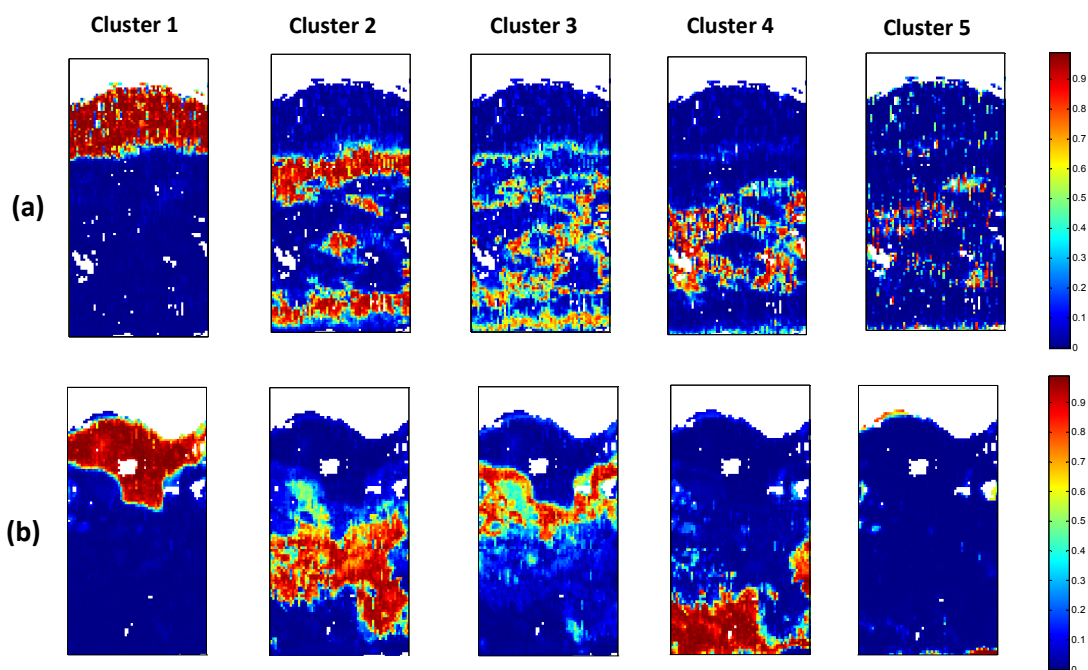


**Figure 2:** FCM clustering on perpendicular polarized FTIR images from untreated (a) and treated with D<sub>2</sub>O (b) 35-year-old skin section. Assignment of the clusters: cluster 1 (epidermis); clusters 2, 3, 4 and 5 (dermis).

Collagen fiber orientation	Young skin samples (35- and 38-year-old)		Old skin samples (60- and 66-year-old)	
	- D <sub>2</sub> O	+ D <sub>2</sub> O	- D <sub>2</sub> O	+ D <sub>2</sub> O
	Parallel	36.7 ± 1.6 %	38.2 ± 2.2 %	39.7 ± 1.2 %
Oblique	38.2 ± 1.9 %	27.5 ± 1.2 %	27.1 ± 2.7 %	26.4 ± 1.7 %
Perpendicular	25.1 ± 2.5 %	34.3 ± 1.6 %	33.2 ± 2.1 %	34.3 ± 1.2 %

**Table 1:** Quantitative analysis of different orientations (parallel, oblique and perpendicular) of collagen fibers in the different-age skin samples, untreated (- D<sub>2</sub>O) and treated (+ D<sub>2</sub>O) with D<sub>2</sub>O. The percentages were calculated from the number of pixels in the clusters associated to the different orientations. Standard deviations were obtained after averaging data collected on 5 analyzed sections for each skin sample.

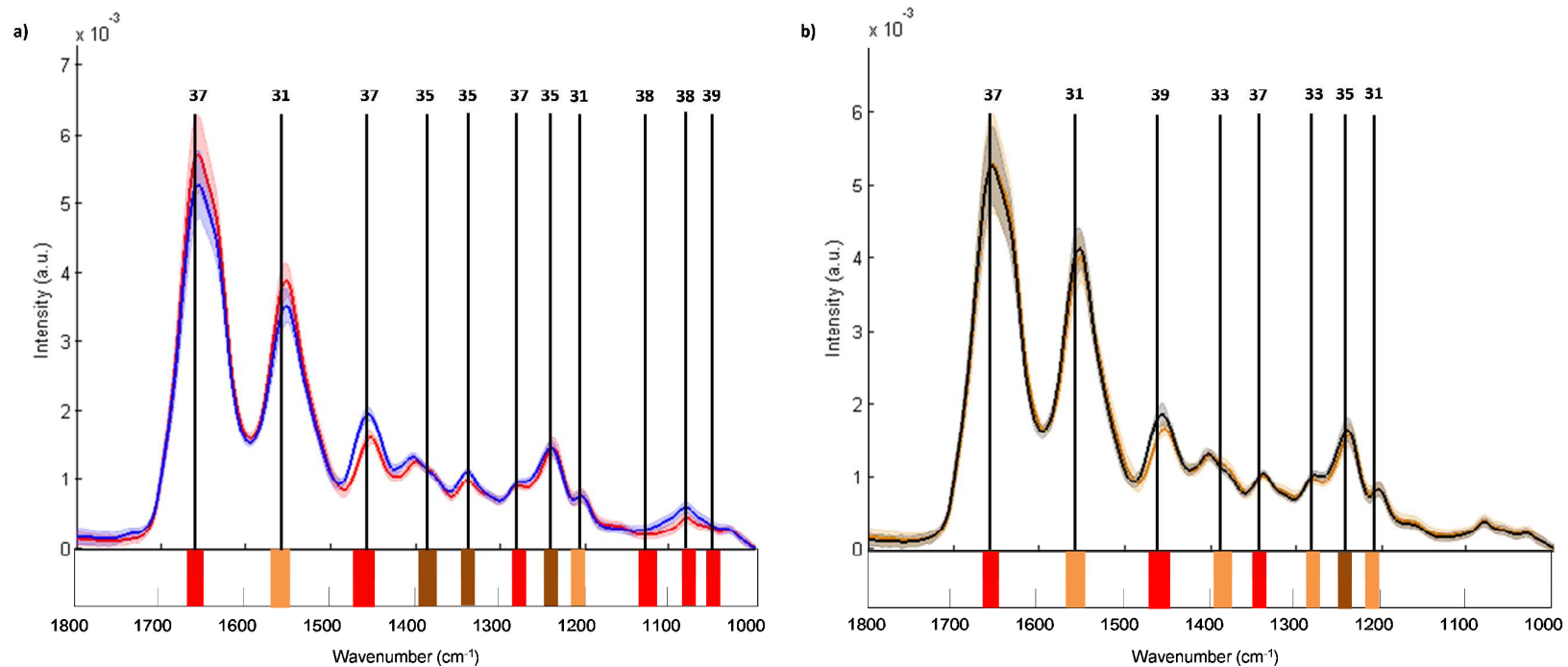


**Figure 3:** Discriminant wavenumbers identified by using randfeatures algorithm in perpendicular oriented collagen fibers, (a) between D<sub>2</sub>O-untreated (*in red*) and treated (*in blue*) 35-years-old dermal skin samples and (b) D<sub>2</sub>O-untreated (*in orange*) and treated (*in black*) 66-years-old dermal skin samples. Respective scores are indicated above color-coded discriminant wavenumbers according to their discrimination level (30-33: orange; 34-36: brown;  $\geq 37$ : red).

Peak position (cm <sup>-1</sup> )	Possible vibrations	Assignments
1650	Amide I (C=O stretch)	Proteins
1550	Amide II (C-N stretch, N-H bend)	Proteins
1455	C-H bend	Proteins
1390	C-H and N-H bend	Proteins
1340	CH <sub>2</sub> wagging	Proteins
1280	Amide III (C-N stretch, N-H bend)	Proteins
1240	Amide III (C-N stretch, N-H bend)	Proteins
1205	Amide III (C-N stretch, N-H bend)	Proteins
1115	C-O stretch, C-O bend	Carbohydrates
1080	C-O stretch, C-O bend	Carbohydrates
1030	C-O stretch, C-O bend	Carbohydrates

**Table 2:** FTIR spectral peak attributions.

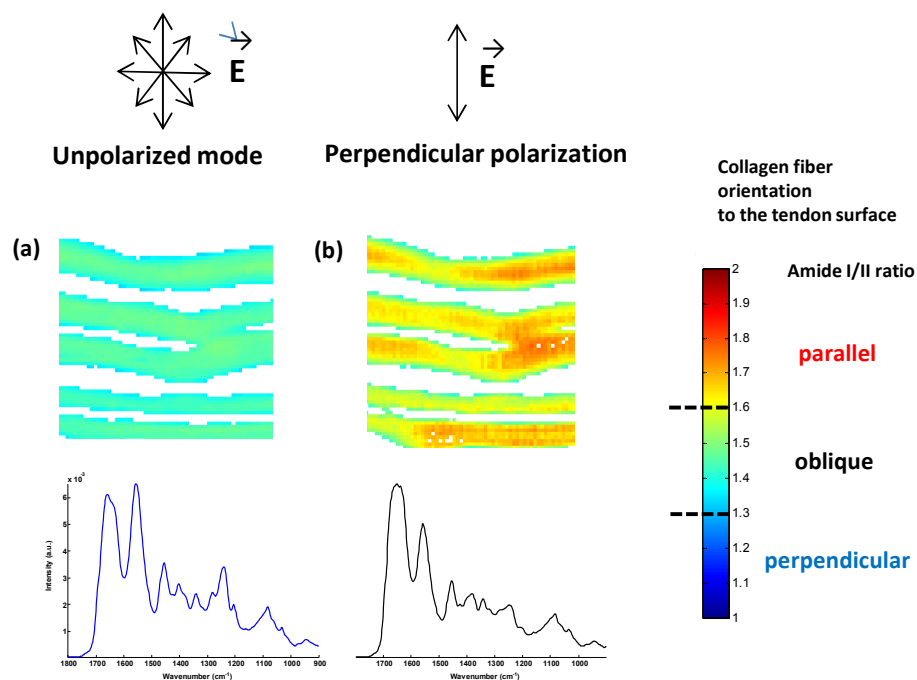


**Figure S1:** FTIR imaging on rat-tail tendon section. Amide I/Amide II (integrated intensities:  $1590\text{-}1720\text{ cm}^{-1}/1480\text{-}1590\text{ cm}^{-1}$ ) ratio-based reconstructed FTIR images and mean spectra in the non-polarized mode (a) and with the perpendicular polarization (b).

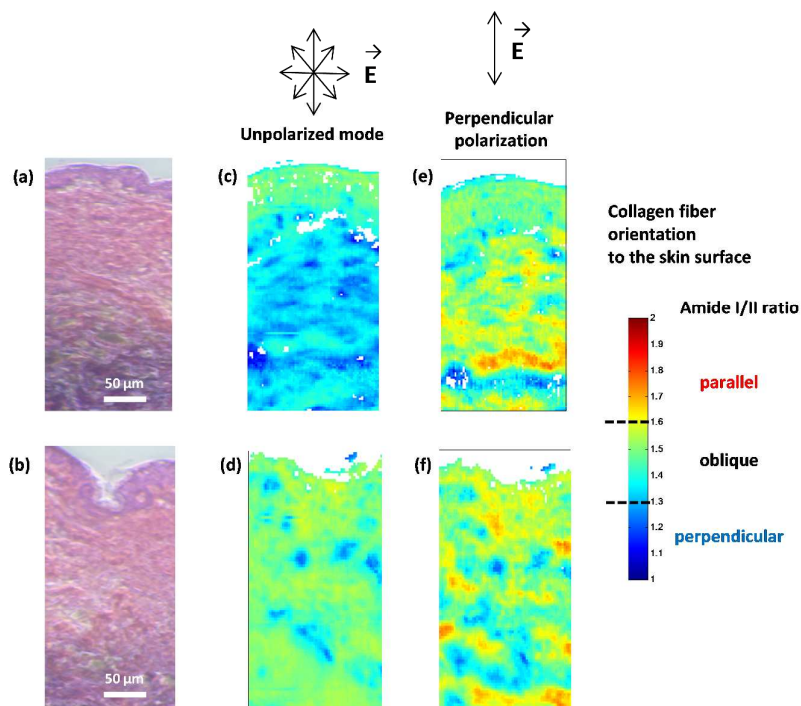


**Figure S2:** FTIR imaging on 38-year-old skin sections treated or not with D<sub>2</sub>O. H&E stained adjacent tissue sections from untreated (a) and treated (b) skin sample. Corresponding Amide I/Amide II (integrated intensities: 1590-1720 cm<sup>-1</sup>/1480-1590 cm<sup>-1</sup>) ratio-based reconstructed FTIR images in the non-polarized mode (c, d) and with the perpendicular polarization (e, f). Scale bar = 50 μm.

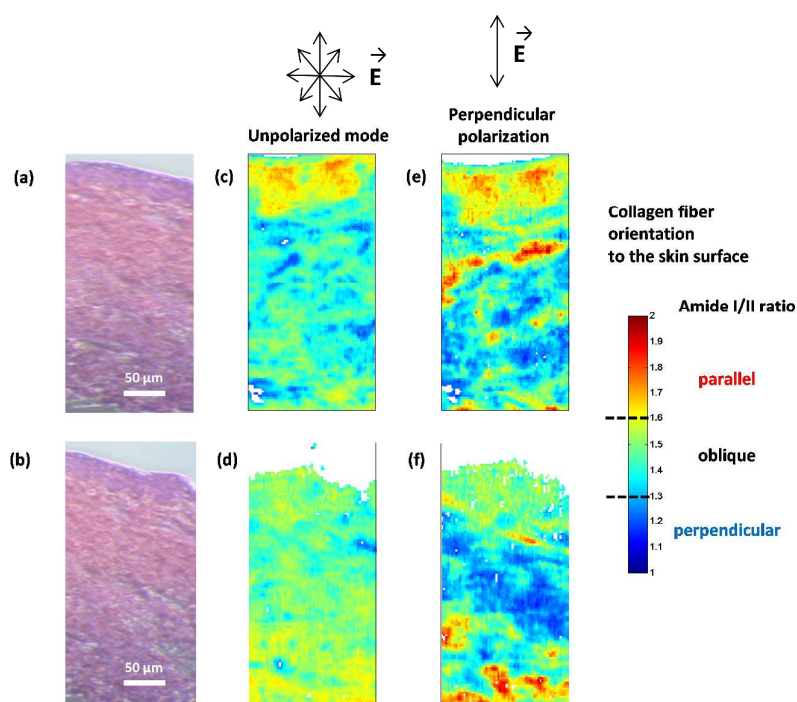


**Figure S3:** FTIR imaging on 60-year-old skin sections treated or not with D<sub>2</sub>O. H&E stained adjacent tissue sections from untreated (a) and treated (b) skin sample. Corresponding Amide I/Amide II (integrated intensities: 1590-1720 cm<sup>-1</sup>/1480-1590 cm<sup>-1</sup>) ratio-based reconstructed FTIR images in the non-polarized mode (c, d) and with the perpendicular polarization (e, f). Scale bar = 50 μm.

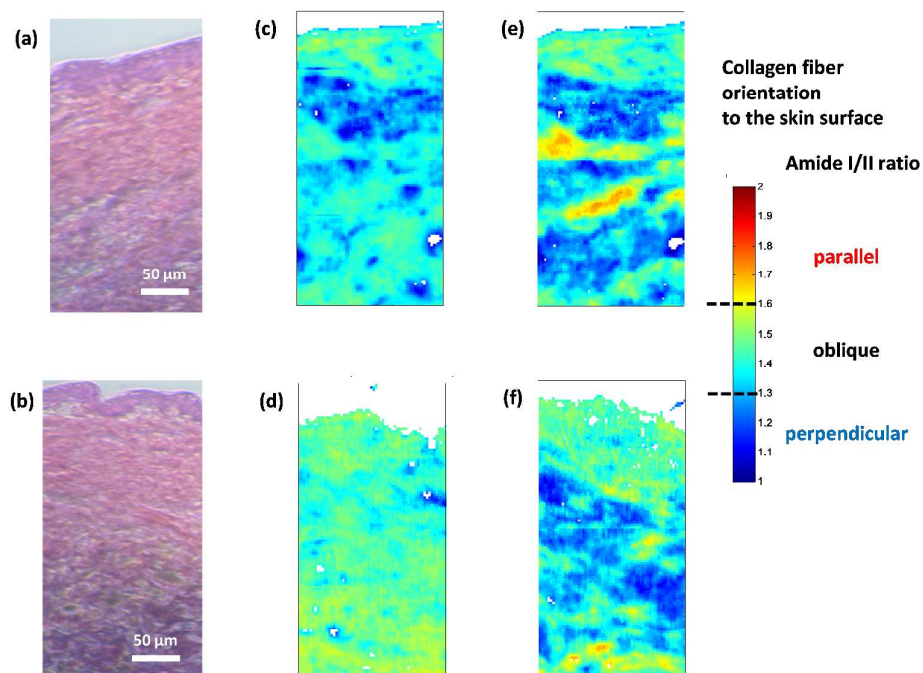


**Figure S4:** FTIR imaging on 66-year-old skin sections treated or not with D<sub>2</sub>O. H&E stained adjacent tissue sections from untreated (a) and treated (b) skin sample. Corresponding Amide I/Amide II (integrated intensities: 1590-1720 cm<sup>-1</sup>/1480-1590 cm<sup>-1</sup>) ratio-based reconstructed FTIR images in the non-polarized mode (c, d) and with the perpendicular polarization (e, f). Scale bar = 50 μm.

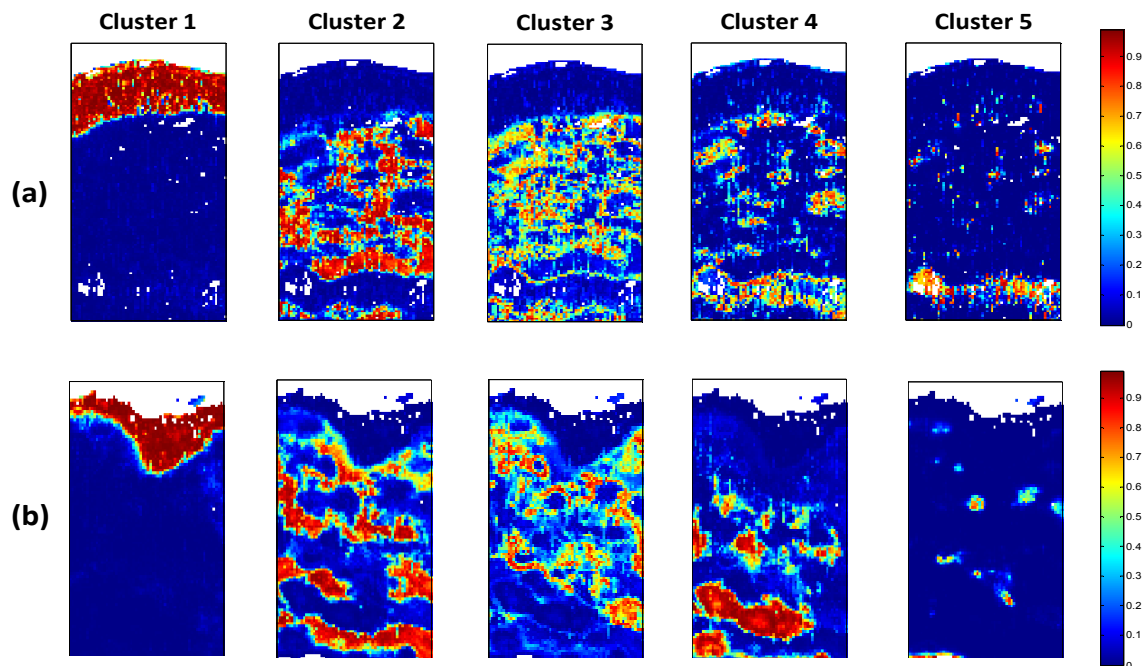


**Figure S5:** FCM clustering on perpendicular polarized FTIR images from untreated (a) and treated with D<sub>2</sub>O (b) 38-year-old skin section. Assignment of the clusters: cluster 1 (epidermis); clusters 2, 3, 4 and 5 (dermis).

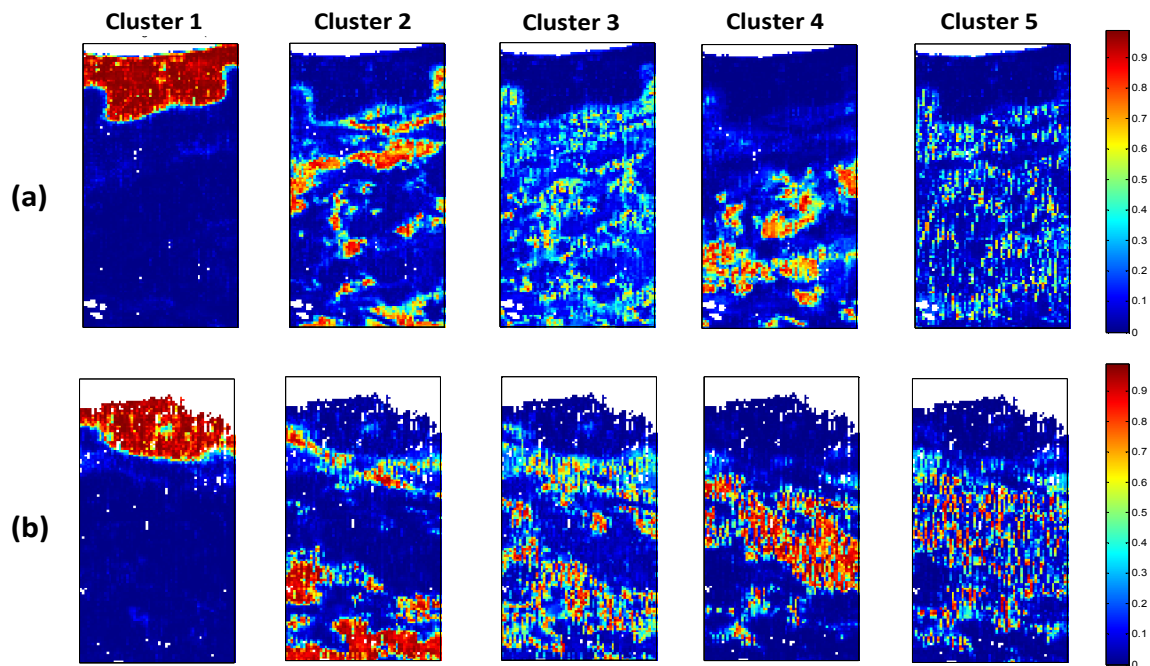


**Figure S6:** FCM clustering on perpendicular polarized FTIR images from untreated (a) and treated with D<sub>2</sub>O (b) 60-year-old skin section. Assignment of the clusters: cluster 1 (epidermis); clusters 2, 3, 4 and 5 (dermis).

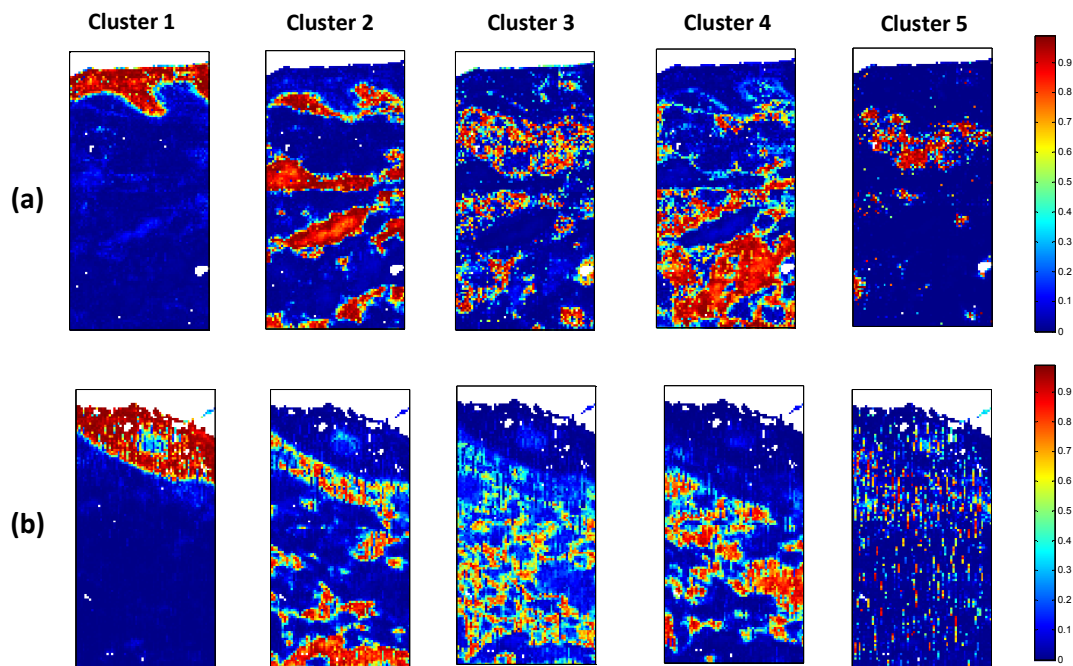


**Figure S7:** FCM clustering on perpendicular polarized FTIR images from untreated (a) and treated with D<sub>2</sub>O (b) 66-year-old skin section. Assignment of the clusters: cluster 1 (epidermis); clusters 2, 3, 4 and 5 (dermis).

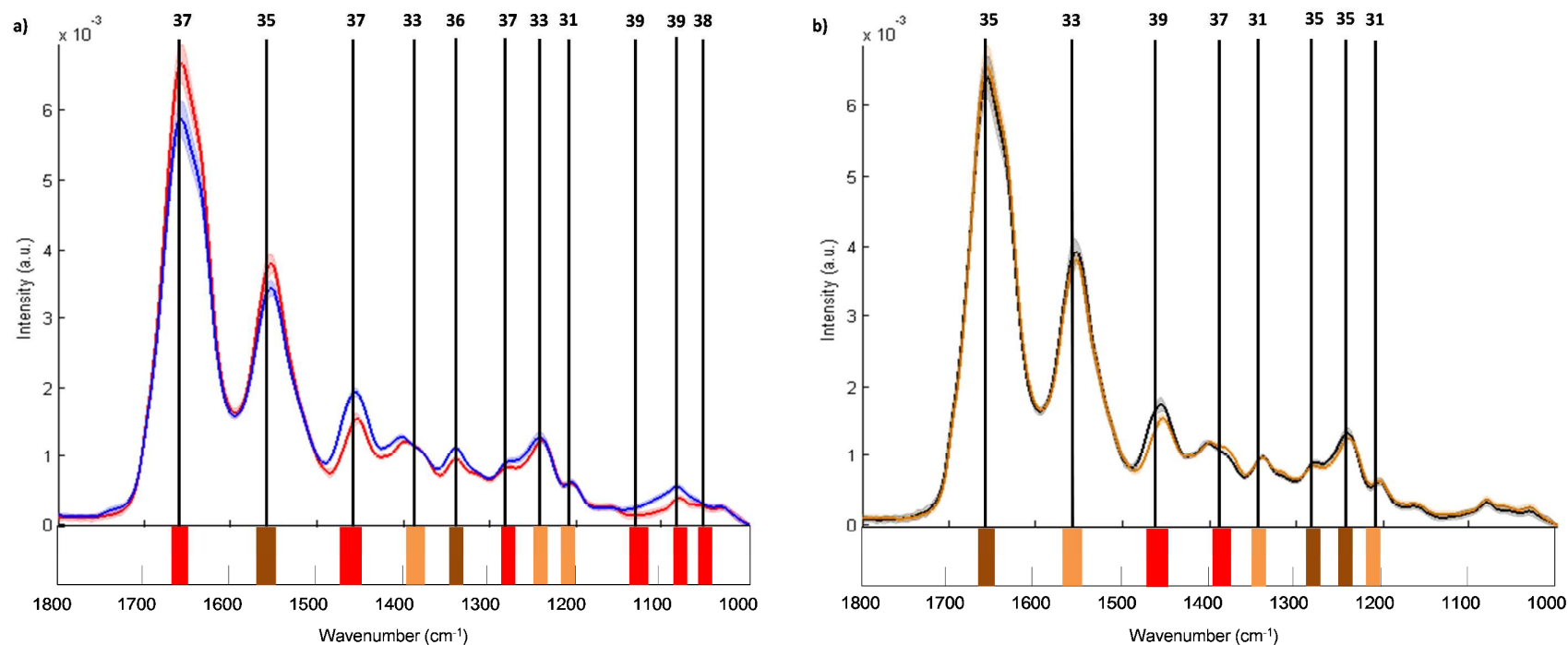


**Figure S8:** Discriminant wavenumbers identified by using randfeatures algorithm in perpendicular oriented collagen fibers, (a) between D<sub>2</sub>O-untreated (*in red*) and treated (*in blue*) 38-years-old dermal skin samples and (b) D<sub>2</sub>O-untreated (*in orange*) and treated (*in black*) 60-years-old dermal skin samples. Respective scores are indicated above color-coded discriminant wavenumbers according to their discrimination level (30-33: orange; 34-36: brown;  $\geq 37$ : red).

1  
2  
3  
4  
5  
6  
7  
8  
9  
10  
11  
12  
13  
14  
15  
16  
17  
18  
19  
20  
21  
22  
23  
24  
25  
26  
27  
28  
29  
30  
31  
32  
33  
34  
35  
36  
37  
38  
39  
40  
41  
42  
43  
44  
45  
46  
47  
48  
49  
50  
51  
52  
53  
54  
55  
56  
57  
58  
59  
60